Ore Geology Reviews 91 (2017) 419–431

Contents lists available at ScienceDirect

Ore Geology Reviews

journal homepage: www.elsevier.com/locate/oregeorev

Sulfide saturation mechanism of the Poyi magmatic Cu-Ni sulfide deposit in Beishan, Xinjiang, Northwest China

Yuegao Liu[a,b], Wenyuan Li[a], Xinbiao Lü[b,*], Yanrong Liu[c], Banxiao Ruan[b], Xiao Liu[b]

[a] Key Laboratory for the Study of Focused Magmatism and Giant Ore Deposits, Ministry of Land and Resources, Xi'an Center of China Geological Survey, Xi'an 710054, China

[b] Institute of Geological Survey, China University of Geosciences, Wuhan 430074, China

[c] College of Earth Science and Resources, Chang'an University, Xi'an 710054, China

ARTICLE INFO

Keywords:
Beishan
Poyi magmatic Cu-Ni sulfide deposit
Sulfide saturation
Multiple sulfur isotopes
Fractional crystallization

ABSTRACT

The Poyi Cu-Ni deposit is hosted by the Early Permian Pobei mafic-ultramafic complex along the northern margin of the Tarim Plate. This series of multiple intrusions in the Poyi deposit can be divided into four lithologies: gabbro, dunite, hornblende peridotite, and wehrlite. The ore body consists mainly of disseminated sulfides hosted by hornblende peridotite. All the Poyi deposit sulfides show positive $\Delta^{33}S$ values from 0.004 to 0.221‰ and negative $\delta^{34}S$ values from −0.8 to −3.5‰. High Ni contents occur in the hornblende peridotites, which exhibit the highest $\Delta^{33}S$ value of 0.221‰ and the lowest $\delta^{34}S$ value of −3.5‰, indicating contamination by sulfides from Archean sedimentary rocks. This contamination was important during sulfide saturation in the Poyi intrusions and likely occurred at depth before the emplacement of the Poyi intrusions. The intrusions incorporated country rocks during their emplacement and consolidation, and the degree of assimilation increases from the central lithofacies (i.e., the hornblende peridotite) to the marginal lithofacies (i.e., the wehrlite, dunite, olivine gabbro, and gabbro). Higher Ni contents are correlated with lower degrees of contamination; thus, we infer that the contamination by the country Paleoproterozoic rocks, which contain significant amounts of gneiss and marble, hindered sulfide saturation.

The whole-rock Ni content is negatively correlated with the MgO and Fo contents in the olivine and positively correlated with the FeO and MnO contents in the olivine. During crystallization, olivine becomes gradually richer in FeO but poorer in MgO, and Mn tends to be enriched in the late stages of the melt. We infer that the fractional crystallization of olivine was an important factor during sulfide saturation.

1. Introduction

Magmatic sulfide deposits are formed by sulfide segregation from mantle-derived mafic-ultramafic magmas (Naldrett, 2004). The distribution coefficient between sulfides and silicates ($D^{Sul/Sil}$) is between 10^3 and 10^5 for platinum group elements (PGEs) (Peach et al., 1990; Stone et al., 1990; Fleet et al., 1991), between 10^2 and 10^3 for Cu, and between 300 and 1000 for Ni (Francis, 1990; Peach et al., 1990). Therefore, Cu, Ni, and PGEs are highly compatible in sulfides. The occurrence of sulfides in silicate melts requires sulfide saturation in the magma system, and the sulfur content at sulfide saturation (SCSS) is influenced by the temperature, pressure, oxygen (fO_2), and magmatic composition (Wendlandt, 1982; Mavrogenes and O'Neill, 1999; Li and Ripley, 2009; Liu et al., 2007; Ripley and Li, 2013).

Li and Ripley (2009) presented an empirical equation for the SCSS based on available experimental results. The SCSS conforms to equation (I), where P is in kbars, T is in Kelvin, X is the mole fraction, and Xi is the mole fraction of the content of oxide i in the melt:

$$\ln X_S = -1.76 - 0.474(10^4/T) - 0.021\,P + 5.559X_{FeO} + 2.565X_{TiO_2} + 2.709X_{CaO} - 3.192X_{SiO_2} + 3.049X_{H_2O} \quad (I)$$

is positively correlated with the contents of FeO, TiO_2, and CaO and negatively correlated with SiO_2

Generally, SCSS is positively correlated with pressure, the content of FeO, TiO_2, CaO, and H_2O and negatively correlated with temperature and the content of SiO_2 (Wendlandt, 1982; Mavrogenes and O'Neill, 1999; Liu et al., 2007; Li and Ripley, 2009). Sulfide saturation in most uncontaminated mantle-derived magmas will not occur via fractional crystallization until ~20–40% crystallization is reached (Ripley and Li, 2013). Previous research suggested that the consumption of FeO during crystallization differentiation is also an important factor in sulfide saturation (Chai et al., 2011; Wykes et al., 2015; Xue et al., 2016). For

* Corresponding author.
E-mail address: luxb@cug.edu.cn (X. Lü).

http://dx.doi.org/10.1016/j.oregeorev.2017.09.013
Received 1 April 2017; Received in revised form 27 August 2017; Accepted 19 September 2017
Available online 23 September 2017

example, the sulfide saturations of PGE-disseminated sulfide deposits, such as the Jinbaoshan deposit and Niquelandia mafic-ultramafic intrusion, and sulfide-poor but PGE-enriched layers, such as those in the Sonju Lake intrusion, are related to the crystal fractionation of olivine and chromite (Ferreira Filho et al., 1995; Miller, 1999; Park et al., 2004; Tao et al., 2007).

Sulfide saturation is both influenced by crystallization differentiation and by contamination with crustal material, especially the addition of crustal sulfur (Lightfoot and Hawkesworth, 1997; Naldrett, 2004; Sun, 2009; Tang et al., 2012; Sharman et al., 2013; Fortin et al., 2015). The combination of $\Delta^{33}S$ and $\delta^{34}S$ values provides a robust method to fingerprint sulfur reservoirs in a wide range of geologic settings (Bekker et al., 2009; Fiorentini et al., 2012a,b; Sharman et al., 2013).

Xue et al. (2016) inferred that the addition of crustal S remains the best explanation for sulfide saturation in initial magma. However, the sulfides in the Poyi Cu-Ni deposit exhibit mantle-like sulfur isotopes ($\delta^{34}S = -0.3$ to $-2‰$) (Xia et al., 2013). Measurements of both $\Delta^{33}S$ and $\delta^{34}S$ are particularly important to detect the importance of Archean S in mafic igneous rocks because many Archean sedimentary rocks do not show $\delta^{34}S$ values that significantly differ from the mantle values, which are near 0‰ (Farquhar et al., 2000; Farquhar and Wing, 2003). Thus, we conducted a field, geochemical, multiple-sulfur-isotope ($\Delta^{33}S$ and $\delta^{34}S$) and olivine-composition study of this intrusion to constrain the effects of fractional crystallization and crustal contamination on sulfide saturation.

2. Geologic setting

Some of the Permian mafic-ultramafic intrusions that were discovered in northern Xinjiang, Northwest China (Fig. 1), host economic magmatic sulfide deposits. Their discovery makes northern Xinjiang the second most important district for Ni resources in China (Mao et al., 2008; Pirajno et al., 2009; Qin et al., 2011; Han et al., 2013). The Cu–Ni deposits along the northeastern margin of the Tarim Basin are mainly distributed in three areas (Fig. 1C): Beishan (Pobei), central Tianshan, and eastern Tianshan (Han et al., 2004; Zhou et al., 2004; Jiang et al., 2006; Chai et al., 2008; Pirajno et al., 2008; Han et al., 2010; Qin et al., 2011; Zhang et al., 2011; Tang et al., 2012).

The Cu–Ni deposits that are related to Early Permian mafic–ultramafic deposits in eastern Tianshan include Huangshandong, Tulargen, Huangshanxi, Hulu, and Xianshan (Fig. 1C). The country rocks mainly belong to Middle Ordovician and Carboniferous strata (Dong et al., 2005).

Central Tianshan formed from a Precambrian block that contained both the Tianyu and Baishiquan Cu–Ni deposits (Fig. 1C). The country rocks of these deposits comprise Paleoproterozoic and Mesoproterozoic strata, which consist mainly of mica-quartz schist and gneiss, with ages of 997 Ma–1829 Ma (Dong et al., 2005).

The Beishan Terrane, where the Poyi Cu-Ni deposit is located, is traditionally considered to be a Paleozoic rift zone (Xiao, 2004; Su et al., 2011). The Beishan rift zone consists of a Precambrian crystalline basement and primarily Paleoproterozoic overlying sedimentary rocks (Xu et al., 2009). The rift zone is separated from the Kruktag Block to the west by the Xingxingxia Fault and from the Dunhuang Block to the east by the Liuyuan Fault (Fig. 1).

The mafic-ultramafic intrusions in the Pobei, such as Luodong, Poshi, Poyi, and Podong, have been successively explored in recent decades (Fig. 1) (Jiang et al., 2006; Li et al., 2006; Yang et al., 2008; Ao et al., 2010; Yang, 2011; Su, 2014; Yang et al., 2014; Liu et al., 2015, 2016; Xue et al., 2016; Zhang et al., 2017). The Pobei mafic-ultramafic complex is approximately 35 km in length and 8 km in width (Fig. 2). This complex mainly consists of three mafic intrusions from the southwest to the northeast: gabbro, magnetite-mineralized gabbro, and leucocratic gabbro (Fig. 2). The Poshi, Poyi, and Podong ultramafic rocks, which hosts the Cu–Ni ore, comprises gabbro intrusions, are enclosed into gabbro intrusions; the Xiaochangshan Fe deposit is exposed in the southern portion of the magnetite-mineralized gabbro (Fig. 2). The Cu-Ni sulfide and Fe-Ti oxide ores in the Pobei area were

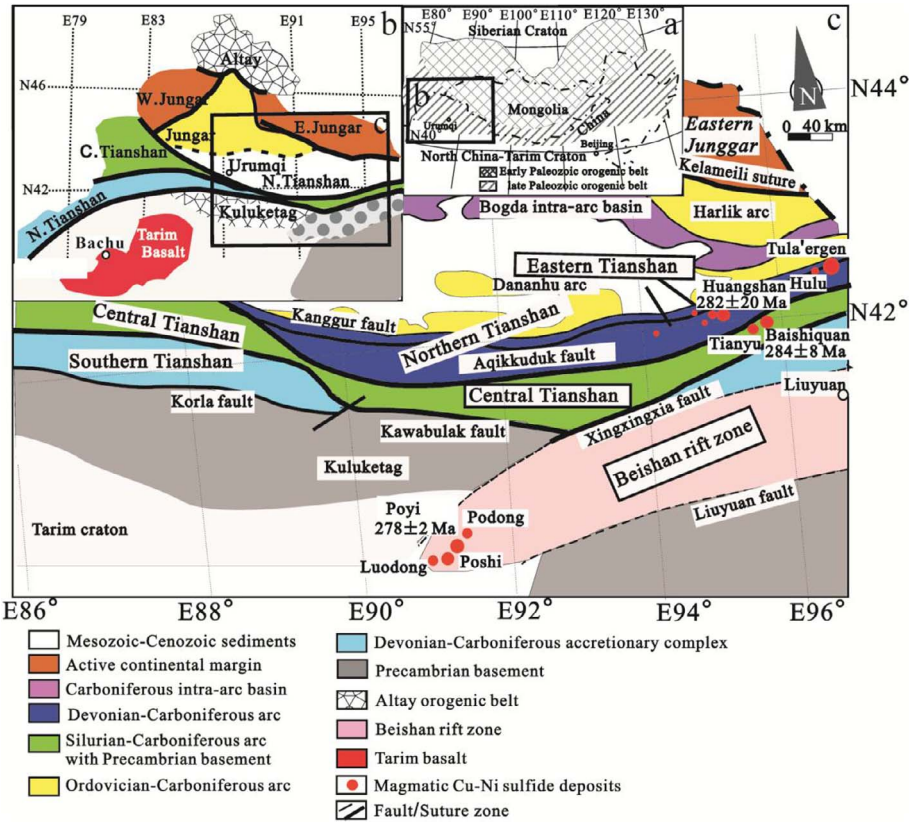

Fig. 1. Tectonic units and distribution of magmatic deposits and Early Permian basalts in northern Xinjiang, Northwest China (modified after BGMRXUAR 1993; Yu et al., 1999; Xiao et al., 2004). Age resources: Mao et al. (2003), Wu et al. (2005), Jiang et al. (2012).

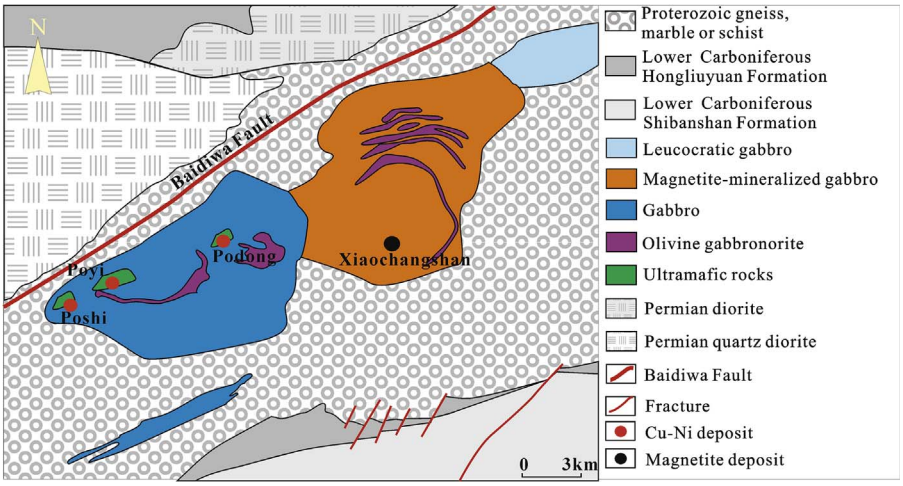

Fig. 2. Geologic map of the Pobei mafic-ultramafic complex (Liu et al., 2017).

products of cogenetic parent magma during the Early Permian (Liu et al., 2017).

The mafic–ultramafic intrusions exhibit close relationships with regional faults. The Baidiwa–Yunihe Fault has had a long-term effect on the distribution of the Pobei mafic–ultramafic intrusions and Cu–Ni deposits. The exposed rocks in the Beishan (Pobei) area include the Proterozoic gneiss, marble or schist; the Lower Carboniferous Hongliuyuan Formation; and the Shibanshan Formation (Xiao, 2004).

3. Geology of the Poyi deposit

The Poyi ultramafic intrusion trends ENE–WSW (Fig. 3) and is 2.8 km long and 2.4 km wide, covering an area of approximately 6.72 km^2. The ultramafic rock phase is 2.2 km long, averages 0.6 km in width, and covers an area of approximately 1.32 km^2. The rocks that surround this intrusion include Paleoproterozoic quartz-biotite schist, gneiss and marble (2203 ± 74 Ma) (Xiao, 2004) (Fig. 2), with some Paleoproterozoic rocks appearing to be large xenoliths in the intrusion (Fig. 3). The lithofacies of the Poyi ultramafic intrusion are dunite, hornblende peridotite, wehrlite, olivine gabbro, and gabbro. The dunite and wehrlite are situated in the center of the intrusion, the gabbro is located at the edge, the olivine gabbro crops out in batholiths in the gabbro lithofacies, and the hornblende peridotite is only observed at depth, as shown in the cross-section in Fig. 4. The dip angle of the Poyi intrusion is approximately 60–70° (Fig. 4). The ore bodies are strictly controlled by the hornblende peridotite that can be classified into marginal and central facies. The ore bodies are located in the central facies (Fig. 4).

The gabbro is located on the periphery of the intrusion, so we speculated that the gabbro was formed earlier in the mafic-ultramafic intrusion. The hornblende peridotite wraps the dunite (Fig. 5A), which suggests that the hornblende peridotite formed later than the dunite. The contact boundary between the hornblende peridotite and wehrlite features a chilled border in the wehrlite (Fig. 5B), confirming that the wehrlite formed later than the hornblende peridotite. Thus, the multiple intrusions of the Poyi deposit formed during four main stages. The intrusion sequence is as follows: gabbro, dunite, hornblende peridotite, and wehrlite.

Dunite is mainly yellow-green in hand specimens (Fig. 4A), and the olivine (Ol) contents are > 90% and locally 95%. The olivine crystals are approximately 2–4 mm in size and exhibit adcumulate to mesocumulate texture (Fig. 6A), elliptical or plate shapes, and fracture development. The pyroxene contents are approximately 5–10% and are mainly clinopyroxene (Cpx). The opaque minerals are chromite (Chr), representing approximately 2–3%. The chromite within olivine grains has a spherical shape and a diameter of approximately 50 μm (Fig. 6A), while the chromite outside the olivine grains has a cubic shape and diameters of approximately 100–150 μm (Fig. 6A).

The hornblende peridotite is dark gray in hand specimens (Fig. 4C–E), with visible porphyritic amphiboles and disseminated sulfides. During the reconnaissance stage of the exploration of the Poyi Cu-Ni deposit, some researchers reported that the ore-bearing rocks were lherzolite (Xia et al., 2013). However, upon further detailed investigation in our systematic study, the ore-bearing rocks are more appropriately described as hornblende peridotite. Olivine grains within the hornblende peridotite are approximately 0.5–3 mm in size, in most cases comprising nearly 80% of the rock. The hornblende content is approximately 10–20%. The hornblende grains are plate shaped and have dimensions of 0.5 × 1 mm, with some reaching 3–4 mm (Figs. 4D and E and 6C and D). Petrographic investigation indicates that the

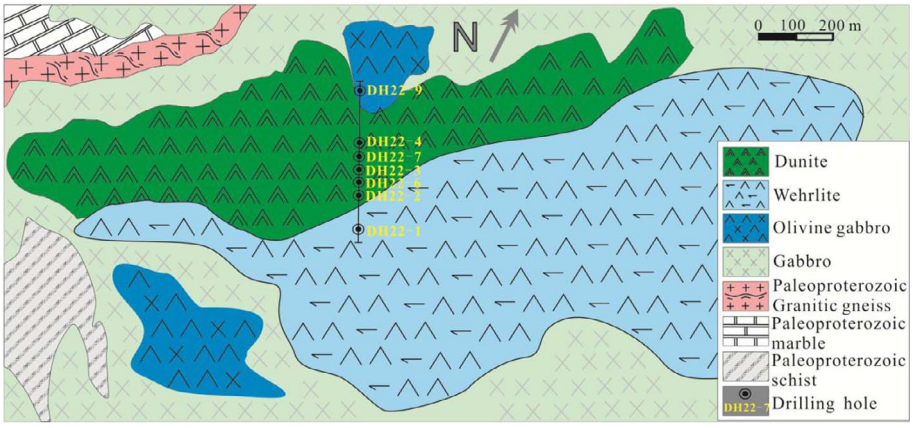

Fig. 3. Geologic map of the Poyi mafic-ultramafic intrusion (modified from SGTXBGMR, 2012).

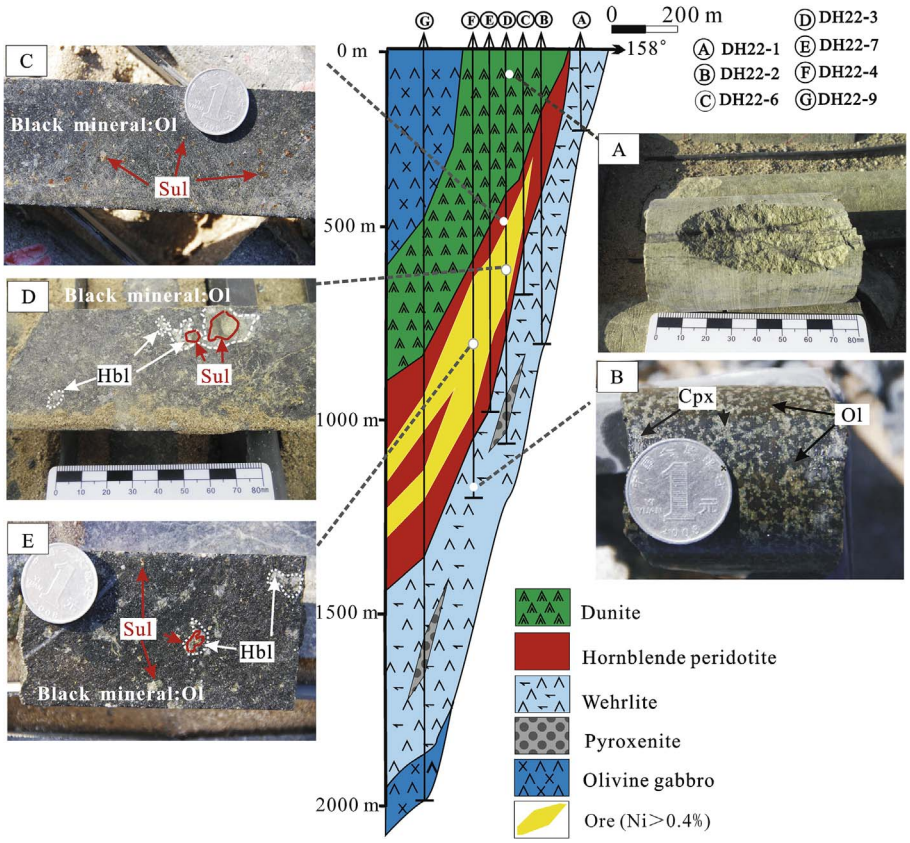

Fig. 4. Lithofacies distribution and ore bodies (Ni > 0.4 wt %) of prospecting line 22 (A: dunite; B: wehrlite; C: marginal facies of the hornblende peridotite; D and E: central facies of the hornblende peridotite).

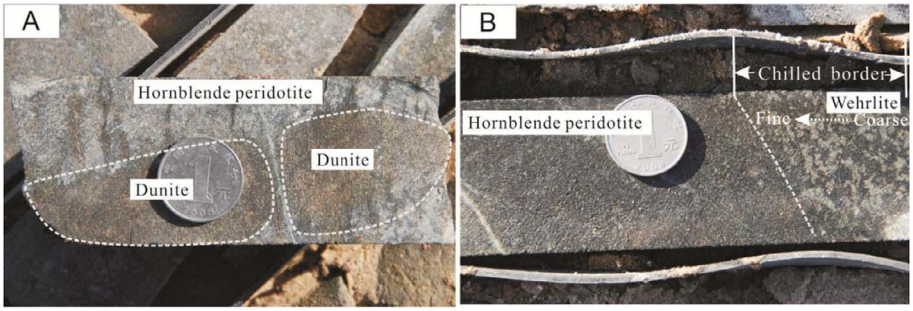

Fig. 5. Contact relationships between the major lithofacies (A: hornblende peridotite that encapsulates dunite; B: chilled border in the wehrlite).

hornblende is the result of the alteration of clinopyroxene (Fig. 6E-1). The orthopyroxene (Opx) and clinopyroxene (Cpx) contents are 2–3% and 5%, respectively. In addition, a small amount of chromite (0.5%) exists. Sulfides (2–4%) mainly include pentlandite (Pn), pyrrhotite (Po), and chalcopyrite (Ccp) (Fig. 6B-D). Sulfides mainly occur in the interstitial space of cumulus olivine (Fig. 6B), with minor sulfides along hornblende cleavage (Fig. 6C and D). We also observed sulfide in the olivine (Fig. 6E-2), chromite (Fig. 6E-3) and boundary between olivine and clinopyroxene (Fig. 6E-2).

The hornblende peridotite can be classified into marginal and central facies. The Ni grade of the marginal facies is mostly lower than 0.4 wt%, and economic ore bodies are mainly distributed in the central facies (Fig. 4). In the marginal facies (Fig. 6C), the hornblende content is lower and the hornblende grains are smaller than those in the central facies of the hornblende peridotite (Fig. 4D and E).

The wehrlite has a fine-grained and cumulate texture (Fig. 4B) and contains Ol (50–65%), which is 2–4 mm in size and oval-shaped, and Cpx (35%) and Opx (5%), which are subhedral columnar in shape and 1–2 mm in size (Fig. 6E). Sulfides (1–2%) are distributed between the olivine and pyroxene (Fig. 6E).

4. Sampling and methods

Geochemical analyses were performed on 156 samples from evenly distributed locations across the seven drill holes from exploratory line No. 22. The sampling interval was between 30 and 40 m, and the Ni, Ti, Ca, and S composition of each sample was analyzed. Geochemical analyses were conducted in the Ministry of Land and Mineral Resources Supervision and Inspection Center of Urumqi (MLMRSICU), China. Ca, Ti, Ni and S were analyzed according to the Geology and Mineral Industry Standard of the People's Republic of China (2016a–c). The detection limits of Ca, Ti, Ni and S were 30 ppm, 5.3 ppm, 0.7 ppm and 8.2 ppm, respectively, and the precision was 0.72%, 0.43%, 1.54% and 2.67%, respectively.

The mineral compositions were determined by using a JXA-8100 electron microprobe at Chang'an University. The analytical conditions included an energy of 15 kV, a beam current of 20 nA, a beam diameter of 1–5 μm and a peak-counting time of 20 s. The analytical error was ± 2‰.

Ten samples with disseminated sulfides from DH22-3 and DH22-4, including five hornblende peridotite, one wehrlite, and four pyroxenite samples, were selected for sulfur isotope analyses ($\delta^{33}S$ and $\delta^{34}S$). The

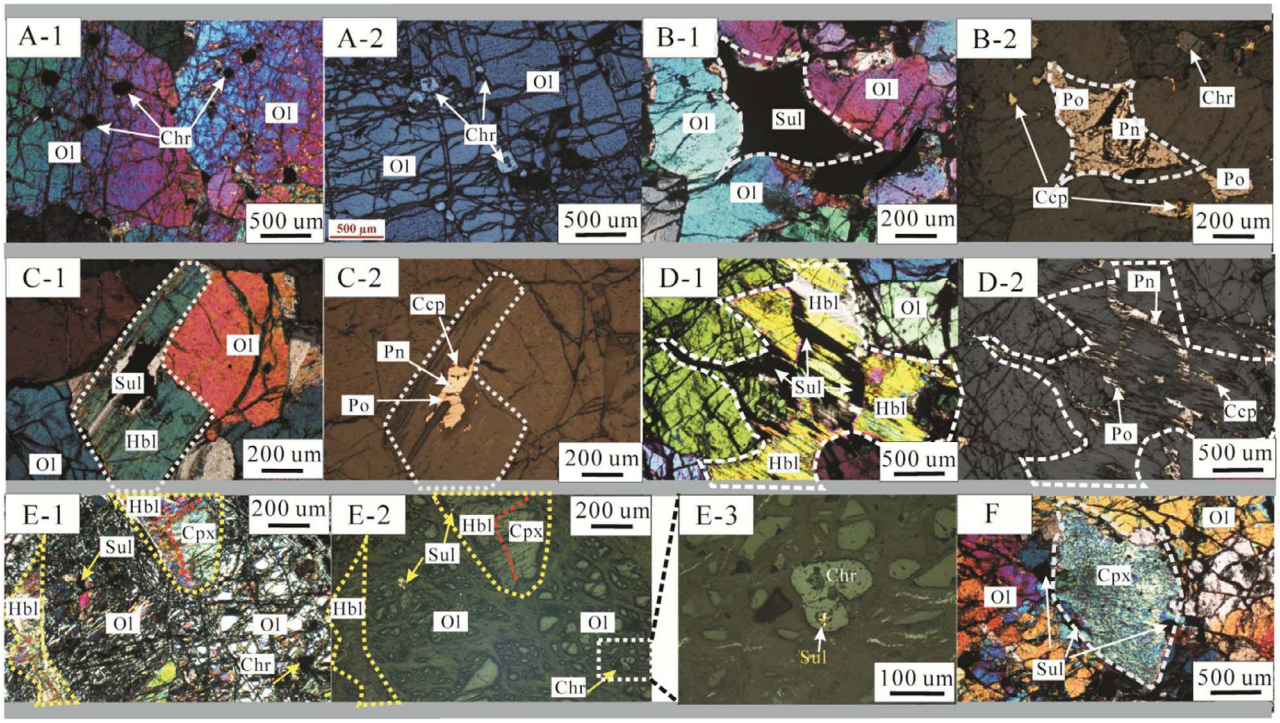

Fig. 6. Photomicrographs of the main rock types. The fields of view in i-1 and i-2 are the same, but i-1 is under transmitted light and i-2 is under reflected light. Ol = olivine, Chr = chromite, Sul = sulfides, Po = pyrrhotite, Pn = pentlandite, Ccp = chalcopyrite, Cpx = clinopyroxene, and Hbl = hornblende. A. Photomicrographs of dunite; sampling location: 105 m in DH22-4. B. Photomicrographs of the marginal facies of hornblende peridotite. Sulfides are mainly present in intergranular olivine. Sampling location: 1068 m in DH22-4. C. Photomicrographs of the marginal facies of hornblende peridotite. A small amount of the sulfides is present in hornblende; the hornblende content is lower and the hornblende particles are smaller than those in the central facies of the hornblende peridotite. Sampling location: 1032 m in DH22-4. D. Photomicrographs of the central facies of hornblende peridotite; sampling location: 870.5 m in DH22-4. E-1. Clinopyroxene that changed to hornblende in hornblende peridotite. Sampling location: 958.8 m in DH22-4. E-2: Sulfide in olivine and the boundary between olivine and clinopyroxene. Sampling location: 958.8 m in DH22-4. E-3: Sulfide in chromite. Sampling location: 958.8 m in DH22-4. F. Photomicrographs of wehrlite. Sampling location: 1688 m in DH22-9.

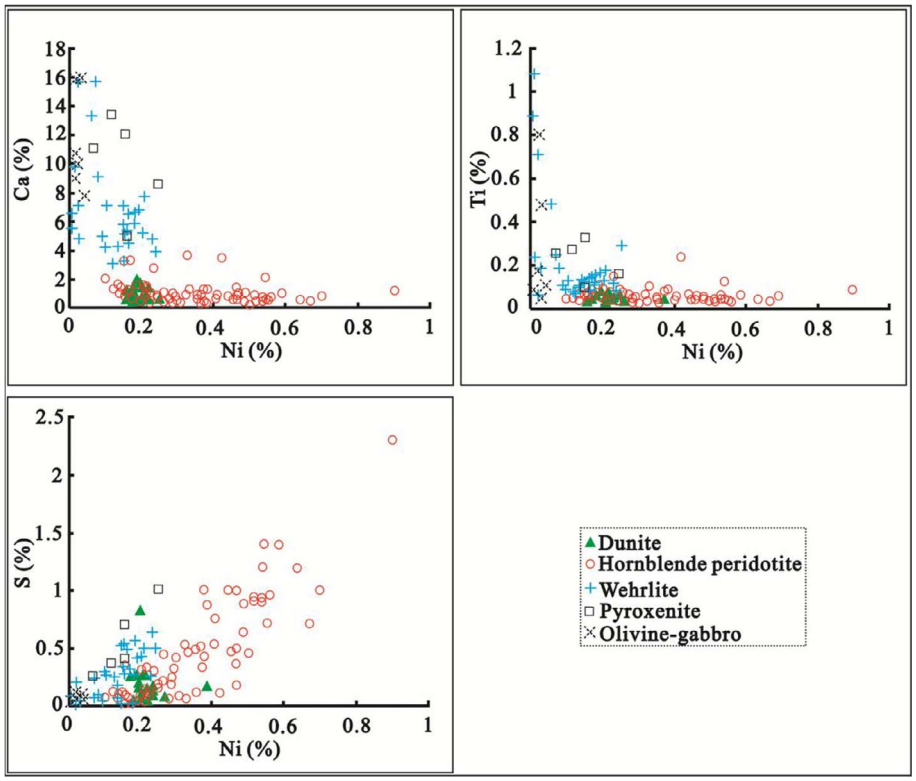

Fig. 7. Relationships between Ni and Ca, Ti, and S in different lithofacies.

whole-rock samples were first pulverized to 100–120 μm in size, and the sulfides were separated from most of the silicate minerals by gravity separation. Then, the sulfides were manually selected under a binocular microscope. The sulfur isotope analyses were conducted in the Beijing Research Institute for Uranium Geology. The method for determining the $\delta^{33}S$ and $\delta^{34}S$ values of the sulfides was as follows. Sulfide minerals and Cu_2O were mixed in fixed proportions and ground to approximately 200 mesh. The mixture was packaged in Cu foil and the mixture was baked for one hour at low temperature under a vacuum environment of 2.0×10^{-2} Pa. The mixture was then heated to a temperature of 980 °C to trigger an oxidation reaction, generating SO_2 gas. Under these vacuum conditions, the SO_2 gas was collected by freezing, and the residue gas was then evacuated by a diffusion pump (Liu et al., 2013). A Delta V Plus gas isotope mass spectrometer was used to determine the SO^+-SO_2^+ sulfur isotopic composition (Baublys et al., 2004). The results are relative to the Canyon Diablo Troilite (CDT) standard and are denoted as $\delta^{34}S_{V\text{-}CDT}$ and $\delta^{33}S_{V\text{-}CDT}$. The analytical precision was better than ± 0.2‰. The sulfide reference materials were the silver sulfide standards GBW-04414 and GBW-04415, which have $\delta^{34}S$ values of −0.07 ± 0.13‰ and 22.15 ± 0.14‰, respectively, and $\delta^{33}S$ values of −0.02 ± 0.11‰ and 11.36 ± 0.14‰, respectively (Ding et al., 2001).

5. Results

5.1. Major elements

The Ni and S contents of the rocks in prospecting line 22 are provided in Supplementary-1.

(1) Relationships between S and Ni

In Fig. 7, S is positively correlated with Ni. Compared to the other lithofacies, the hornblende peridotite exhibits the highest S content. The average S contents in the dunite, hornblende peridotite, wehrlite, pyroxenite, and olivine gabbro are 0.16%, 0.48%, 0.25%, 0.54%, and 0.06%, respectively. The mean Ni values in the dunite, hornblende peridotite, wehrlite, pyroxenite, and olivine gabbro are 0.20%, 0.35%, 0.12%, 0.15%, and 0.02%, respectively. All the dunite samples nearly did not contain any sulfide, so the 0.2% Ni value represents the nickel silicate content. With an average S content of 0.16%, the dunite still did not reach sulfide saturation, so the lower limit of the SCSS value for dunite is 0.16%.

(2) Ni contents of the rocks in drill hole 22-7

The Ni content in drill hole 22-7 is illustrated in Fig. 8, and the detailed data are provided in Supplementary-2. The location of the drill hole is shown in Figs. 3 and 4. In drill hole 22-7, 0–498 m is dunite and 498–961 m is hornblende peridotite. The whole-rock Ni content of the dunite gradually increases from 0.18% at 12.9 m to 0.39% at 498 m. The whole-rock Ni content of the hornblende peridotite is between 0.3 and 0.4% from 498 to 600 m, greater than 0.4% from 600 to 815 m, and between 0.2 and 0.3% at depths greater than 815 m. The depth ranges from 498 to 600 m and from 800 to 960 m feature the marginal facies of the hornblende peridotite, whereas the depth range from 600 to 815 m features the central facies. The central facies is characterized by Ni enrichment. In Fig. 8, the whole-rock Ni content is negatively correlated with the MgO and Fo contents and positively correlated with the FeO and MnO contents in the olivine.

5.2. Mineral compositions

The compositions of olivine are provided in Supplementary-3. We deleted small part of samples that were affected by alteration or granitic veins.

The stratigraphic variations in the olivine Fo, MgO, FeO, SiO_2, and MnO contents in drill hole 22-7 are illustrated in Fig. 8. The location of the drill hole is shown in Figs. 3 and 4.

The olivine Fo in the dunite gradually decreases from 89.7 at 38.8 m to 87.3 at 448.8 m, and the MgO and NiO contents of the olivine decrease with depth from 48.35 to 46.89% and from 0.4% to 0.25%, respectively. In contrast, the FeO content increases with depth from 9.68 to 11.88%, and the SiO_2 and MnO contents do not change with depth. The SiO_2 content of the olivine in the dunite remains at approximately 41%. The Fo and NiO contents of the olivine have a good positive correlation in the dunite. Both values show a progressive decrease downward the stratigraphic section. The whole-rock Ni and olivine NiO have a negative correlation.

In the hornblende peridotite, the olivine Fo and the MgO and NiO contents decrease from the marginal facies to the central facies, whereas the FeO, SiO_2, and MnO contents in the olivine increase from the marginal facies to the central facies (Fig. 8). The whole-rock Ni content in the hornblende peridotite has a negative correlation with the Fo and a positive correlation with the FeO, SiO_2 and MnO in the olivine.

5.3. Multiple sulfur isotopes

The $\delta^{34}S$ values (all the values that are shown here are relative to the Vienna Canyon Diablo Troilite (V-CDT) and expressed in per mil, ‰) of the central hornblende peridotite range from −2.6 to −3.5‰ and average −3‰ (Table 1 and Fig. 9). The $\Delta^{33}S$ values vary between 0.004 and 0.146‰, with an average of 0.063‰. The $\delta^{34}S$ values of the marginal hornblende peridotite range from −0.8 to −1.4‰, with an average of −1.1‰, and the $\Delta^{33}S$ values vary between 0.112 and 0.221‰, with an average of 0.167‰. The $\delta^{34}S$ of the marginal hornblende peridotite is relatively different from the mantle-source $\delta^{34}S$ value (−1.80‰ to 0.49‰; see Gao and Thiemens, 1993; Labidi et al., 2013) compared to the central hornblende peridotite (Fig. 9). However, the $\Delta^{33}S$ value of the central hornblende peridotite is higher than that of the marginal hornblende peridotite (Fig. 9).

The wehrlite has a $\delta^{34}S$ value (Table 1 and Fig. 9) of −2.4 and a $\Delta^{33}S$ value of 0.037‰. The pyrrhotite in the pyroxenite (Table 1 and Fig. 9) has $\delta^{34}S$ values between −1.5 and −2‰, with an average of −1.8‰, and $\Delta^{33}S$ values between 0.073 and 0.131‰, with an average of 0.102‰. The $\delta^{34}S$ values of the chalcopyrite range between −0.8 and −1.7‰, with an average of −1.3‰. Generally, the chalcopyrite has higher $\delta^{34}S$ values than the pyrrhotite, and the $\Delta^{33}S$ values of the chalcopyrite are between 0.012 and 0.076‰.

All the sulfides from the Poyi deposit exhibit positive $\Delta^{33}S$ values between 0.004 and 0.221‰ (Table 1 and Fig. 9). The hornblende peridotite, which has the greatest Ni enrichment, has the highest $\Delta^{33}S$ value (0.221‰).

6. Discussion

6.1. Source of sulfur

The $\delta^{34}S$ values of the central hornblende peridotites range from −2.6 to −3.5‰ (Fig. 9) and average −3‰. These values are significantly lower than typical mantle values (from −1.80‰ to +0.49‰; see Gao and Thiemens, 1993; Labidi et al., 2013), which is strong evidence that crustal sulfur was added to the Poyi deposit. The hornblende peridotites have the highest Ni and S contents. These rocks also exhibit the highest $\Delta^{33}S$ value of 0.221‰ and the lowest $\delta^{34}S$ value of −3.5‰, so the contamination of crustal sulfur was critical to the sulfide saturation in Poyi. However, the rocks that surround the Poyi deposit, including Paleoproterozoic quartz-biotite schist, gneiss and marble, do not contain sulfides. Consequently, what was the source of the crustal sulfur? We attempt to answer this question by using the $\Delta^{33}S$ values of the sulfides in the Poyi deposit.

Multiple sulfur isotopes can be fractionated during both biological

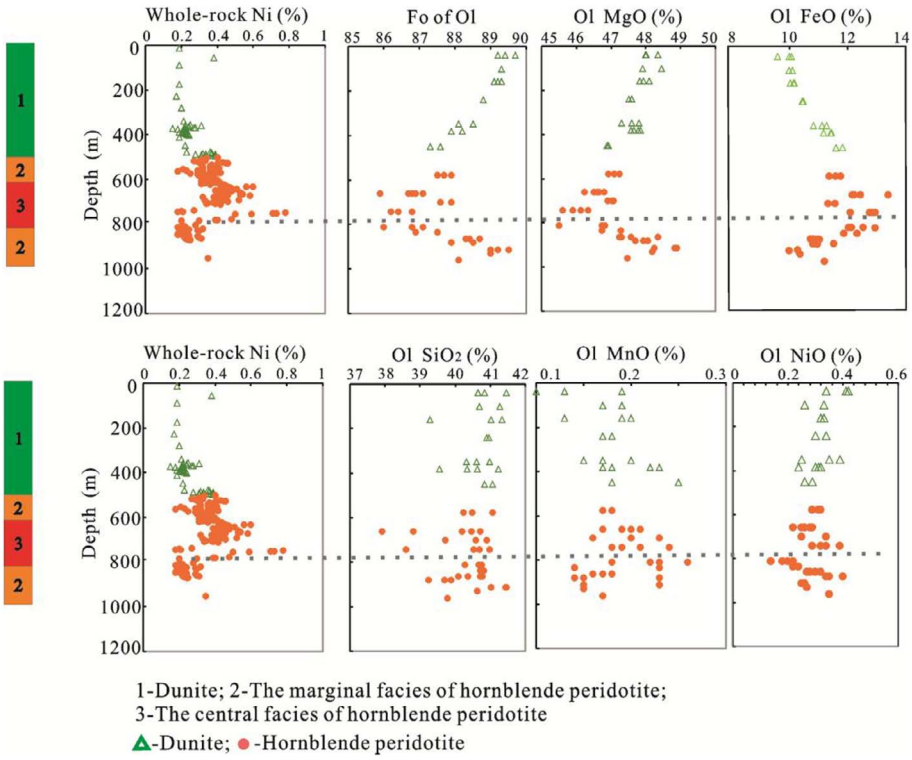

Fig. 8. Relationship between the olivine composition and Ni content of whole rocks in drill hole 22-7.

and inorganic processes on Earth, such that $^{33}S/^{32}S = 1/2\ ^{34}S/^{32}S$ (Hulston and Thode, 1965). The fractionations that obey these rules are described as "mass dependent" (Rumble, 2005). However, Archean sedimentary rocks do not follow this relationship (Farquhar et al., 2000; Bekker et al., 2009), and this deviation in isotopic abundances is called "mass-independent" fractionation (MIF). Volcanic SO_2 gas was photochemically fractionated in the oxygen-poor and ozone-free Archean atmosphere. The nuclear reaction with photons produced an excess of ^{33}S. In the absence of rapid re-oxidation, this process led to an excess of reduced ^{33}S species. Consequently, oxidized and reduced species of sulfur were delivered to the land and oceans without becoming entirely homogenized. Thus, the sulfur isotopes in Archean sedimentary rocks retain a mass-independent signal (Farquhar et al., 2001). The magnitude of this anomalous isotopic fractionation can be characterized by the measurement of $\delta^{33}S$ values ($\delta^{33}S = [(^{33}S/^{32}S)_{sample}/(^{33}S/^{32}S)_{standard} - 1] \times 1000$) and $\delta^{34}S$ values ($\delta^{34}S = [(^{34}S/^{32}S)$ sample/$(^{34}S/^{32}S)$standard $- 1] \times 1000$) and is indicated by nonzero $\Delta^{33}S$ values (δ^{33}Smeasured $- \delta^{33}$Spredicted, where δ^{33}Spredicted $= [(\delta^{34}\text{Smeasured} + 1)^{0.515} - 1] \times 1000$) (Farquhar and Wing, 2003). The $\Delta^{33}S$ values in peridotite xenoliths are zero ($\Delta^{33}S \approx 0.00 \pm 0.03$‰), indicating zero Archean crustal assimilation (Farquhar et al., 2002). However, samples with sulfur that cycled through the Archean surface environment have $\Delta^{33}S$ values above 0.03‰ because the Archean atmosphere was poor in oxygen and free of ozone (leading to an excess of ^{33}S), whereas non-Archean samples do not have $\Delta^{33}S$ values significantly above 0.03‰ (Farquhar and Wing, 2003; Lyons, 2007; Danielache et al., 2008; Watanabe et al., 2009). Thus, $\Delta^{33}S$ values provide a robust and reliable proxy for the assimilation of Archean sediment in magmatic systems. This approach has been applied to the Bushveld Complex, the Voisey's Bay Ni-Cu sulfide deposit, and Ni sulfides that are hosted in komatiites and Ni-Cu-(PGE) deposits in the Tati greenstone belt (Bekker et al., 2009; Ding et al., 2012; Fiorentini et al., 2012a,b; Hiebert et al., 2013; Penniston-Dorland et al., 2012; Sharman et al., 2013).

All the sulfides in the Poyi deposit have positive $\Delta^{33}S$ values between 0.004 and 0.221‰ (Table 1). The hornblende peridotites are most enriched in Ni and exhibit the highest $\Delta^{33}S$ value of 0.221‰, probably indicating that the crustal sulfur originated from Archean sedimentary rocks. Compared to the sulfides in the marginal hornblende peridotite, the sulfides in the central hornblende peridotite have

Table 1
Multiple sulfur isotopes.

Sample Location	Lithofacies	Object	$\delta^{33}S_{V\text{-}CDT}$ (‰)	Average	$\delta^{34}S_{V\text{-}CDT}$ (‰)	Average	$\Delta^{33}S$(‰)	Average
DH22-3 495.5 m	Central hornblende peridotite	Po + Pn	−1.8	−1.5	−3.5	−3	0.004	0.063
DH22-4 805.6 m			−1.4		−3		0.146	
DH22-7 870.1 m			−1.3		−2.6		0.04	
DH22-4 1032.7 m	Marginal hornblende peridotite	Po + Pn	−0.3	−0.4	−0.8	−1.1	0.112	0.167
DH22-3 689 m			−0.5		−1.4		0.221	
DH22-3 1045 m	Wehrlite	Po + Pn	−1.2	−1.2	−2.4	−2.4	0.037	0.037
DH 22-3 1030 m	Pyroxenite	Ccp	−0.4	−0.6	−0.8	−1.3	0.012	0.044
DH22-3 1013.5 m			−0.8		−1.7		0.076	
DH22-3 1030 m		Po	−0.7	−0.8	−1.5	−1.8	0.073	0.102
DH22-3 1013.5 m			−0.9		−2		0.131	

Note: Po-pyrrhotite; Pn-Pentlandite; Ccp-Chalcopyrite.

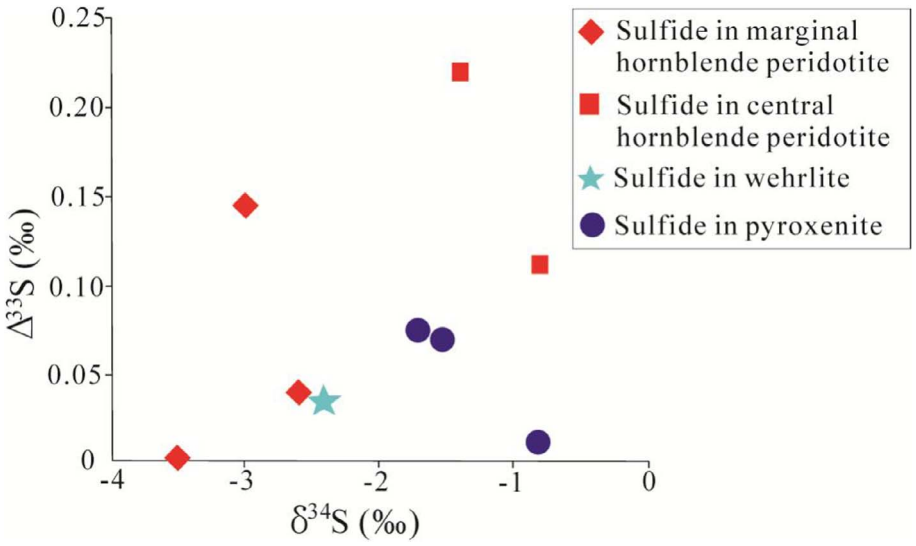

Fig. 9. Plot of $\delta^{34}S$ vs. $\Delta^{33}S$.

relatively higher $\Delta^{33}S$ values (Fig. 9). However, the $\delta^{34}S$ of the marginal hornblende peridotite is more unlike mantle sulfur. Thus, determining which lithofacies contaminated more sulfur among the central hornblende peridotite and the marginal hornblende peridotite is difficult. What we can judge is that some of the crustal sulfur in the Poyi mafic-ultramafic intrusion originated from Archean sedimentary rocks. The rocks that surround the Poyi deposit do not contain Archean sedimentary rocks, so the addition of sulfur from Archean sedimentary rocks should have occurred before the emplacement and consolidation of the Poyi intrusions. This process also occurred in the Bushveld Complex. Penniston-Dorland et al. (2012) demonstrated that the sulfur contamination occurred prior to the emplacement of the Bushveld Complex in the upper crust and that possible sources of contamination included the lower crust and the sub-continental lithospheric mantle.

Water-insoluble reduced sulfur species, such as elemental sulfur, carry a positive $\Delta^{33}S$ signature, having transferred to disseminated sulfides in the Archean sedimentary rocks (Fiorentini et al., 2012a). In contrast, water-soluble oxidized sulfur species (e.g., sulfate) usually have a negative $\Delta^{33}S$ signature (Fiorentini et al., 2012a), and sulfate in seawater generally has $\delta^{34}S$ values from +10‰ to 30‰ (Zheng and Chen, 2000). The hornblende peridotite and pyroxenite have positive $\Delta^{33}S$ values and negative $\delta^{34}S$ values, so the possibility of sulfur contamination from seawater or sulfate can be ruled out. Hence, the Poyi intrusions were probably contaminated by sulfides from deep Archean sedimentary rocks prior to emplacement and consolidation instead of sulfate.

6.2. Crustal contamination

Based on the sulfur isotopes, the Poyi intrusions were likely contaminated by sulfides from Archean sedimentary rocks at depth before emplacement and consolidation. However, what effect did the mixing of the surrounding rocks during the emplacement and consolidation of the Poyi intrusions have on the sulfide saturation? The rocks that surround these intrusions include Paleoproterozoic quartz-biotite schist, gneiss and marble (Xiao, 2004). To determine the influence of Paleoproterozoic gneiss contamination on the sulfide saturation, this study compiled the Sr and Nd isotopes of the different lithofacies from previous studies of the Poyi intrusion (Jiang et al., 2006; Qin and Li, 2011; Yang, 2011; Xia et al., 2013) (Please see Supplementary-4), calculated the average value, and calculated the degree of assimilation of the Paleoproterozoic rock by using a two-end-member isotope-mixing model (Fig. 10). The end members were the Paleoproterozoic gneiss, an Nd content of 29.36 ppm, an $^{143}Nd/^{143}Nd$ ratio (t = 276 Ma) of 0.509762, an Sr content of 721.77 ppm, and an $^{87}Sr/^{86}Sr$ ratio (t = 276 Ma) of 0.712561 (Feng et al., 1995; Hu et al., 1997); and the depleted mantle (DM), which had an Nd content of 23 ppm (Sun and McDonough, 1989), an $^{143}Nd/^{143}Nd$ ratio of 0.5131, an Sr content of 155 ppm, and an $^{87}Sr/^{86}Sr$ ratio of 0.7027 (Salters and Stracke, 2004). The degree of assimilation gradually increased in the hornblende peridotite, wehrlite, dunite, olivine gabbro, and gabbro (Fig. 10). Lithofacies with higher Ni contents had lower degrees of contamination. Thus, Paleoproterozoic gneiss contamination likely played a role in depressing sulfide saturation. The assimilation of Archean sediments with sulfide prior to emplacement and consolidation may have also influenced the Sr-Nd isotope composition. However, if the Archean sediments were the main component that the Poyi intrusion contaminated, the hornblende peridotite should have had the lowest sulfur content because the hornblende peridotite had the lowest contamination among the several lithofacies in Poyi. However, the hornblende peridotite had the highest sulfur content, so the degree of mixing with the Archean sediments was small and the two-end-member isotope-mixing model could generally reflect the contamination degree.

Samples with Ni contents above 0.4 wt% had low Ca (< 2 wt%) and Ti (< 0.1 wt%) contents in the Poyi mafic-ultramafic intrusion (Fig. 7). These results are consistent with the detrimental effects of the addition of calcium and titanium on sulfide saturation in a magmatic system (Liu et al., 2007; Li and Ripley, 2009). The marginal lithofacies of the Poyi intrusion, such as the gabbro and olivine gabbro, had much higher Ca and Ti contents, which may be one reason that those lithofacies did not reach sulfide saturation. Marble is present in the Paleoproterozoic rocks in the Poyi mining area (Fig. 3). The gabbro is in direct contact with the marble (Fig. 11A), and calcite is commonly associated with pyroxene grains in the pyroxenite (Fig. 11B). Thus, the Poyi mafic-ultramafic rocks assimilated some marble. The assimilation of carbonate decreases the sulfide solubility of magmas (Holwell et al., 2007; Lehmann et al., 2007). Generally, the marginal lithofacies should have a higher contamination degree. The hornblende peridotite is located in the center of the intrusions (Fig. 4), which is perhaps an important reason for the sulfide saturation in the hornblende peridotite.

Based on the above evidence, the Poyi intrusions were likely contaminated with sulfides from Archean sedimentary rocks at depth before emplacement and consolidation. This sulfide addition was important for the Poyi intrusion to reach sulfide saturation. However, the incorporation of the country rocks during the emplacement and consolidation of the Poyi intrusions depressed the sulfide saturation.

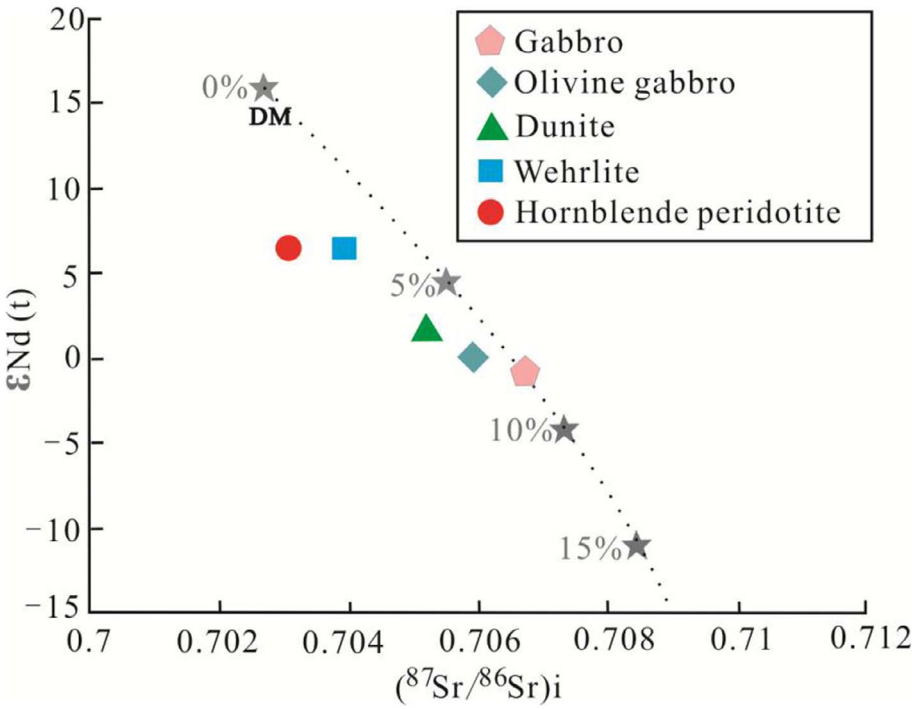

Fig. 10. Quantitative simulation of the degree of contamination by Paleoproterozoic gneiss rocks in different lithofacies in the Poyi Cu–Ni deposit. The gabbro data are from Xia et al. (2013) and Yang (2011) (n = 6), the olivine gabbro data are from Yang (2011) and Jiang et al. (2006) (n = 10), the wehrlite data are from Yang (2011) (n = 1), the hornblende peridotite data are from Xia et al. (2013) (n = 1), and the dunite data are from Qin and Li (2011) (n = 4). The Sr and Nd data are provided in Supplementary-4.

6.3. Fractional crystallization

The increase in the S concentration of a melt because of the crystallization of olivine, pyroxene, feldspar, and other minerals may lead to the separation of so-called "cotectic" proportions of sulfide liquid (Ripley and Li, 2013). Sulfide-poor but PGE-rich layers, such as those in the Sonju Lake intrusion (Miller, 1999; Park et al., 2004), are thought to result from the fractional crystallization of a tholeiitic melt. The whole-rock Ni content is negatively correlated with the NiO content in olivine (Fig. 8). This phenomenon was likely caused by the presence of sulfides during crystallization because Ni preferentially entered the sulfides, with the distribution coefficient between olivine and silicate magma (2.86–13.6) (Takahashi, 1978) being far less than that between a sulfide melt and silicate magma (300–1000) (Barnes and Maier, 1999).

Tao et al. (2007) proposed that sulfide saturation was reached because of olivine and chromite crystallization in the magma, thereby producing PGE-enriched disseminated sulfide zones in the Jinbaoshan intrusion in China. During crystallization, the olivine became gradually richer in FeO but poorer in MgO. The distribution coefficient for Mn between olivine and a basaltic melt is 0.42–0.917 (Bougault and Hekinian, 1974; Ohtani et al., 1989), so Mn tends to be enriched in the late stage of the melt. In Fig. 7, the whole-rock Ni content was negatively correlated with the MgO and Fo contents and positively correlated with the FeO and MnO contents in the olivine. Therefore, the whole-rock Ni content had a close relationship with the crystallization of olivine. We infer that the fractional crystallization of olivine was also an important factor during sulfide saturation.

We also used the MELTS program by Ghiorso and Sack (1995) and Asimow and Ghiorso (1998) to estimate the relationship between the fractional crystallization of olivine and the SCSS. The parental magma's composition and primary temperature were required for this purpose. We used the method of Chai and Naldrett (1992), the composition of the most primitive olivine (i.e., Fo = 89.7) among the selected samples, the olivine liquid Fe-Mg exchange coefficient [Kd, $(FeO/MgO)_{Ol}/(FeO/MgO)_{Liq}$] of 0.3 ± 0.03 by Roeder and Emslie (1970), and the average composition of the selected samples from Song et al. (2011), Xia et al. (2013), Liu (2015) and found that the MgO and FeO contents in the parental magma were 14.26 wt% and 6.28 wt%, respectively. We could draw a best-fit line through the relationship between each major element and MgO based on the major element data for the selected samples. Then, we could calculate the original content of each major element based on a primary MgO content of 9.26 wt%. Thus, we could determine the liquid composition of the parental magma (all in wt%): MgO = 14.26, FeO = 6.28, Fe_2O_3 = 0.83, SiO_2 = 49.44, Al_2O_3 = 13.56, CaO = 10.98, K_2O = 0.28, MnO = 0.11, Na_2O = 2.11, Cr_2O_3 = 0.06, P_2O_5 = 0.03, NiO = 0.05, TiO_2 = 0.58 and LOI = 1.45.

The above calculations indicated the composition of the parental

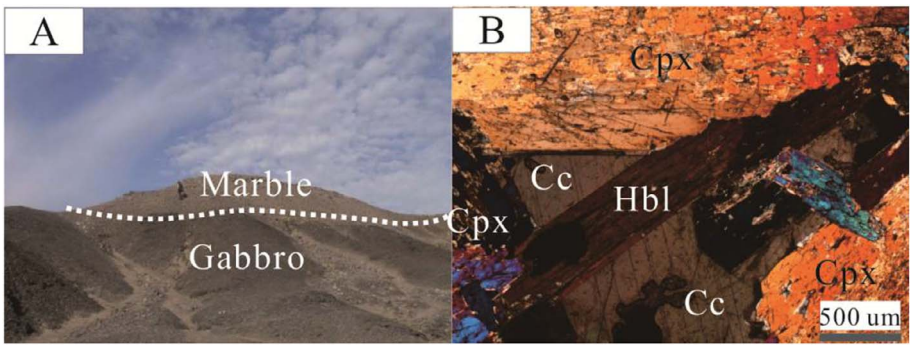

Fig. 11. Evidence for the contamination of a carbonate component in the Poyi mafic-ultramafic intrusions (A: gabbro in direct contact with marble; B: calcite in pyroxenite; Cpx: clinopyroxenes; Hbl: hornblende; Cc: Calcite).

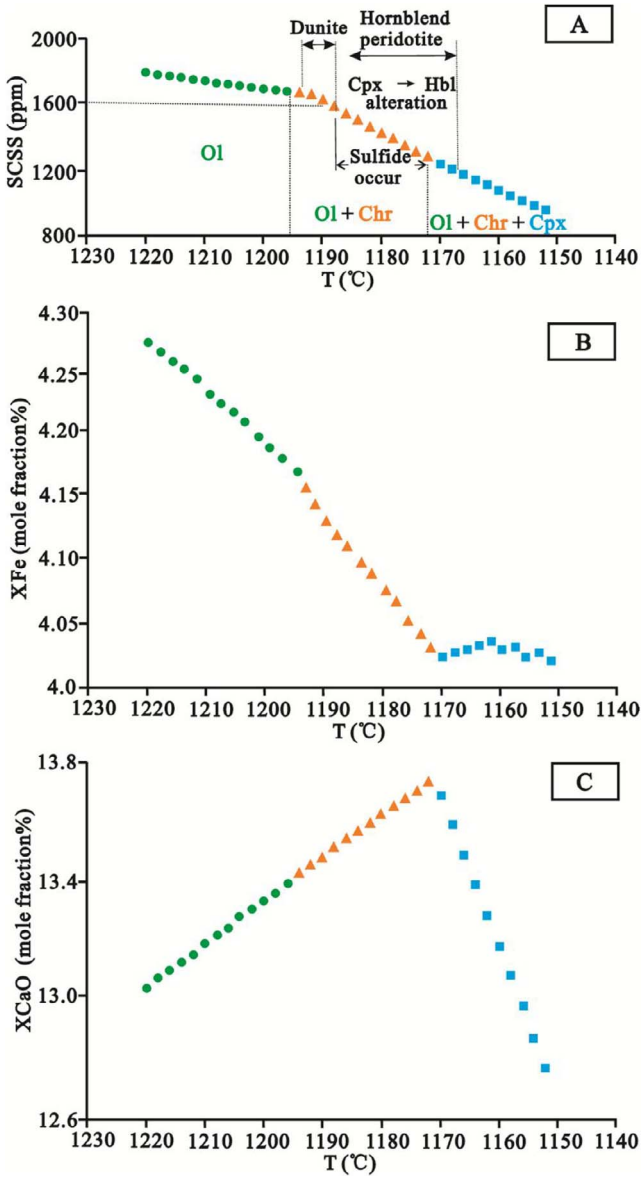

Fig. 12. Model of the variation in the sulfur contents at sulfide saturation (SCSS) during fractional crystallization. The modeling details were provided in the text. Ol = olivine, Chr = chromite, Cpx = clinopyroxene.

magma. Then, we calculated the crystallization temperature of the olivine with the highest Fo to be 1217 °C by using the formula by Roeder and Emslie (1970), i.e., log $(X_{Ol}MgO)/(X_{liq}MgO) = 3740/T - 1.87$, where T is in Kelvin and X is the mole fraction.

We used the liquid composition of the parental magma and a fixed logf O_2 of FMQ +1 and pressure of 1 kbar in the Melts program to simulate fractional crystallization between 1217 °C (the primary temperature) and 1150 °C (Fig. 12).

In Fig. 12-A, the sole crystalline phase from 1220 °C to 1196 °C was olivine, while chromite and clinopyroxene occurred at 1194 °C and 1170 °C, respectively. Sulfides mainly occurred in the interstitial space of cumulus olivine (Fig. 6B) and in the olivine (Fig. 6E-2), chromite (Fig. 6E-3) and boundary between the olivine and clinopyroxene (Fig. 6E-2) in the hornblende peridotite, indicating that sulfide saturation occurred during the crystallization of olivine and chromite but before the crystallization of clinopyroxene. The lack of sulfides in dunite indicates that the magma was not sulfide-saturated when dunite crystallized. The dunite experienced the cotectic crystallization of olivine and chromite, and the average sulfur content in the dunite was 1600 ppm. We inferred the location of the dunite and hornblende in our model based on this information, as shown in Fig. 12. The crystallization of chromite caused the SCSS to drop faster (Fig. 12-A), which should have been caused by the crystallization of chromite leading to a slightly faster drop in the Fe mole fraction (X_{Fe}) in the residual melt (Fig. 12-B). The clinopyroxene crystallization increased the X_{Fe} from 1170 °C to 1178 °C (Fig. 12-B). This increase in X_{Fe} created a higher SCSS, but the crystallization of the clinopyroxene had no influence on the SCSS (Fig. 12-A). The clinopyroxene crystallization rapidly decreased the CaO mole fraction in the residual melt (Fig. 12-C). This reduction in the X_{CaO} was beneficial to the SCSS drop, which probably counteracted the effect of the increase in X_{Fe} on the SCSS. Fig. 12 shows that the SCSS was greatly influenced by the crystallization of olivine and chromite, which is consistent with our idea that the fractional crystallization of olivine was an important factor during sulfide saturation in the Poyi Cu-Ni deposit.

6.4. Metallogenic model for Poyi Cu-Ni deposit

Below, we summarize a metallogenic model for the Poyi Cu-Ni deposit, which contains a small amount of sulfides (Fig. 13), based on the above evidence:

(1) The country rocks do not contain sulfides.
(2) The compositions of the country rocks hindered sulfide saturation.
(3) The Cu-Ni deposits generally contain disseminated ore.

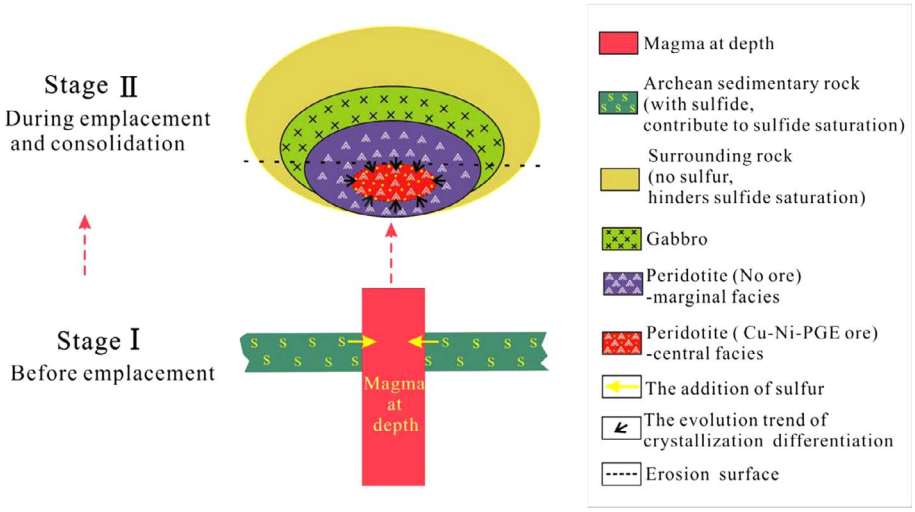

Fig. 13. Metallogenic model for the Poyi Cu-Ni deposit.

The main characteristics of this model are as follows (Fig. 13):

(1) This model can be divided into two stages. Prior to the emplacement of the Poyi intrusions, the magma was contaminated with sulfides from Archean sedimentary rocks, which was an important factor during sulfide saturation in the Poyi intrusions. The second stage occurred during the emplacement and consolidation of the Poyi intrusions and involved the incorporation of country rocks, which hindered sulfide saturation.
(2) The peripheral rocks for the Poyi intrusions are gabbros, whereas the central rocks are peridotite, which were less contaminated by the country rocks. The peridotite can be divided into central and marginal facies, and the degree of crystallization differentiation increases from the marginal facies to the central facies. Additionally, disseminated ore mainly occurs in the central facies of the peridotite. Relative to the olivine in the central facies, the olivine in the marginal facies has higher MgO and Fo contents and lower FeO and MnO contents.

7. Conclusions

(1) All the sulfides in the Poyi deposits showed positive $\Delta^{33}S$ values from 0.004 to 0.221‰ and negative $\delta^{34}S$ values from −0.8 to −3.5‰. The hornblende peridotites had the highest Ni contents. These rocks also exhibited the highest $\Delta^{33}S$ value of 0.221‰ and the lowest $\delta^{34}S$ value of −3.5‰, indicating contamination by sulfides from Archean sedimentary rocks. This factor was important during the sulfide saturation of the Poyi intrusions. This contamination probably occurred at depth before the emplacement of the Poyi intrusions. During the emplacement and consolidation of these intrusions, the incorporation of the country rocks hindered sulfide saturation.
(2) The whole-rock Ni content was negatively correlated with the MgO and Fo contents and positively correlated with the FeO and MnO contents in the olivine. The sulfide saturation of the Poyi Cu-Ni deposit was closely related to the crystallization of olivine and chromite.

Acknowledgments

We are very grateful to the Associate Editor Peter C. Lightfoot, Dr. Cesar F. Ferreira Filho and Dr. Xueming Yang for their great help in improving the manuscript. This study was financially supported by the project of the Pobei Cu-Ni Sulfide Deposits Metallogenic Regularity and Location Prediction of Rich Ores of Xinjiang Province (Grant XGMB2012012), the National Science and Technology Support Plan 305 project in Xinjiang (2011BAB06B04-0), the State Scholarship Fund ([2016]3035-201608610016) from the China Scholarship Council, the China Postdoctoral Science Foundation (2015M582762XB), the China Geological Survey Project (DD20160013), the Integration and Service of the Mineral Geology and Metallogenic Regularity in China (DD20160346), and the 1:50000 geological survey of J46E020013, J46E021013, and J46E022013 in the Lalinggaolihe area of Golmud in Qinghai (121201011000150005-19).

Appendix A. Supplementary data

Supplementary data associated with this article can be found, in the online version, at http://dx.doi.org/10.1016/j.oregeorev.2017.09.013.

References

Ao, S.J., Xiao, W.J., Han, C.M., Mao, Q.G., Zhang, J.E., 2010. Geochronology and geochemistry of Early Permian mafic-ultramafic complexes in the Beishan area, Xinjiang, NW China: implications for late Paleozoic tectonic evolution of the southern Altaids. Gondwana Res. 18 (2–3), 466–478.

Asimow, P.D., Ghiorso, M.S., 1998. Algorithmic modifications extending MELTS to calculate subsolidus phase relations. Am. Mineral. 83, 1127–1132.

Barnes, S.J., Maier, W., 1999. The fractionation of Ni, Cu and the noble metals in silicate and sulphide liquids. Geological Association of Canada Short Course Notes 13, 69–106.

Baublys, K.A., Golding, S.D., Young, E., Kamber, B.S., 2004. Simultaneous determination of $\delta^{33}S_{V\text{-}CDT}$ and $\delta^{34}S_{V\text{-}CDT}$ using masses 48, 49 and 50 on a continuous flow isotope ratio mass spectrometer. Rapid Commun. Mass Spectrom. 18, 2765–2769.

Bekker, A., Barley, M.E., Fiorentini, M.L., Rouxel, O.J., Rumble, D., Beresford, S.W., 2009. Atmospheric sulfur in Archean komatiite-hosted nickel deposits. Science 326 (5956), 1086–1089.

Bougault, H., Hekinian, R., 1974. Rift Valley in the Atlantic Ocean near 36°50′N: petrology and geochemistry of basaltic rocks. Earth Planet. Sci. Lett. 24, 249–261.

Bureau of Geology and Mineral Resources of Xinjiang Uygur Autonomous Region (BGMRXUAR), 1993. Regional Geology of Xinjiang Uygur Autonomous Region. Geological Publishing House, Beijing pp 841. (in Chinese).

Chai, F., Zhang, Z., Mao, J., Dong, L., Zhang, Z., Wu, H., 2008. Geology, petrology and geochemistry of the Baishiquan Ni–Cu-bearing mafic–ultramafic intrusions in Xinjiang, NW China: implications for tectonics and genesis of ores. J. Asian Earth Sci. 32 (2–4), 218–235.

Chai, F.M., Xia, F., Chen, B., Lu, H.F., 2011. Characteristics Research on Chromite from the Poyi Cu-Ni Sulfide-bearing Mafic-ultramafic Intrusions in the Beishan Block, Xinjiang. J. Xinjiang Univ. (Nat. Sci. Ed.) 28, 389–394 (in Chinese with English abstract).

Chai, G., Naldrett, A.J., 1992. The Jinchuan ultramafic intrusion: cumulate of a high-Mg basaltic magma. J. Petrol. 33 (2), 277–303.

Danielache, S.O., Eskebjerg, C., Johnson, M.S., Ueno, Y., Yoshida, N., 2008. High-precision spectroscopy of 32S, ^{33}S, and ^{34}S sulfur dioxide: ultraviolet absorption cross sections and isotope effects. J. Geophys. Res. Atmos. (1984–2012) 113 (D17), 277–303.

Ding, T.P., Vaikiers, S., Wan, D.F., Bai, R.M., Zou, X.Q., Li, Y.H., Zhang, Q.L., Bievre, P., 2001. The $\delta^{33}S$ and $\delta^{34}S$ values and absolute $^{33}S/^{32}S$ and $^{33}S/^{34}S$ ratios of IAEA and Chinese sulfur isotope reference materials. Bull. Mineral. Petrol. Geochem. 20 (4), 425–427 (in Chinese with English abstract).

Ding, X., Ripley, E.M., Shirey, S.B., Li, C., 2012. Os, Nd, O and S isotope constraints on country rock contamination in the conduit-related Eagle Cu–Ni–(PGE) deposit, midcontinent rift system, Upper Michigan. Geochim. Cosmochim. Acta 89 (4), 10–30.

Dong, L.H., Cui, B., Qu, X., He, Z.J., Liu, T., Sang, S.J., Wang, W.J., Han, C.M., Bai, G.Y., Guo, H.X., 2005. Location Prediction and evaluation of copper deposits in the middle part of Eastern Tianshan. pp. 268. (in Chinese).

Farquhar, J., Bao, H., Thiemens, M., 2000. Atmospheric influence of Earth's earliest sulfur cycle. Science 289 (5480), 756–758.

Farquhar, J., Savarino, J., Airieau, S., Thiemens, M.H., 2001. Observation of wavelength-sensitive mass-independent sulfur isotope effects during SO_2 photolysis: implications for the early atmosphere. J. Geophys. Res. Planets (1991–2012) 106 (E12), 32829–32839.

Farquhar, J., Wing, B., McKeegan, K., Harris, J., Cartigny, P., Thiemens, M., 2002. Mass-independent sulfur of inclusions in diamond and sulfur recycling on early Earth. Science 298 (5602), 2369–2372.

Farquhar, J., Wing, B.A., 2003. Multiple sulfur isotopes and the evolution of the atmosphere. Earth Planet. Sci. Lett. 213 (1), 1–13.

Feng, B.Z., Zhou, Y.W., Chi, S.F., 1995. Presinian Geology, precious and nonferrous metal deposits in Kuruketage area, Xinjiang Uygur autonomous region, China. Geological Publishing House, Beijing pp 282. (in Chinese).

Ferreira Filho, C.F., Naldrett, A.J., Asif, M., 1995. Distribution of platinum-group elements in the Niquelandia layered mafic-ultramafic intrusion, Brazil: implications with respect to exploration. Can. Mineralogist 33, 165–184.

Fiorentini, M., Beresford, S., Barley, M., Duuring, P., Bekker, A., Rosengren, N., Cas, R., Hronsky, J., 2012a. District to camp controls on the genesis of komatiite-hosted nickel sulfide deposits, Agnew-Wiluna greenstone belt, Western Australia: insights from the multiple sulfur isotopes. Econ. Geol. 107 (5), 781–796.

Fiorentini, M.L., Bekke, r.A., Rouxel, O., Wing, B.A., Maier, W., Rumble, D., 2012b. Multiple sulfur and iron isotope composition of magmatic Ni-Cu-(PGE) sulfide mineralization from eastern Botswana. Econ. Geol. 107 (1), 105–116.

Fleet, M., Stone, W., Crocket, J., 1991. Partitioning of palladium, iridium, and platinum between sulfide liquid and basalt melt: effects of melt composition, concentration, and oxygen fugacity. Geochim. Cosmochim. Acta 55 (9), 2545–2554.

Fortin, M.A., Riddle, J., Desjardins-Langlais, Y., Baker, D.R., 2015. The effect of water on the sulfur concentration at sulfide saturation (SCSS) in natural melts. Geochim. Cosmochim. Acta 160, 100–116.

Francis, R.D., 1990. Sulfide globules in mid-ocean ridge basalts (MORB), and the effect of oxygen abundance in Fe-S-O liquids on the ability of those liquids to partition metals from MORB and komatiite magmas. Chem. Geol. 85 (3), 199–213.

Gao, X., Thiemens, M.H., 1993. Variations of the isotopic composition of sulfur in enstatite and ordinary chondrites. Geochim. Cosmochim. Acta 57 (13), 3171–3176.

Geology and Mineral Industry Standard of People 's Republic of China, 2006a. Analysis Methods for Regional Geochemical Sample-Part 1: Determination of Aluminum Oxide etc. 24 Components by Pressed Power Pellets-X-ray Fluorescence Spectrometry. pp 1–11. (in Chinese).

Geology and Mineral Industry Standard of People 's Republic of China, 2006b. Analysis Methods for Regional Geochemical Sample-Part 3: Detrmination of Barium, Beryllium, Bismuth etc. 15 Elements Content by Inductively Coupled Plasma Mass Spectrometry. pp 1–12. (in Chinese).

Geology and Mineral Industry Standard of People 's Republic of China, 2006c. Analysis Methods for Regional Geochemical Sample-Part 28: Determination of Sulfur by Burning – Iodine Quantity Method. pp 1–5. (in Chinese).

Ghiorso, M.S., Sack, R.O., 1995. Chemical mass transfer in magmatic processes IV. A revised and internally consistent thermodynamic model for the interpolation and extrapolation of liquid-solid equilibria in magmatic systems at elevated temperatures and pressures. Contrib. Miner. Petrol. 119 (2–3), 197–212.
Han, B., Ji, J., Song, B., Chen, L., Li, Z., 2004. SHRIMP zircon U-Pb ages of Kalatongke No. 1 and Huangshandong Cu-Ni-bearing mafic-ultramafic complexes, North Xinjiang, and geological implications. Chin. Sci. Bull. 49 (22), 2424–2429.
Han, C., Xiao, W., Zhao, G., Ao, S., Zhang, J., Qu, W., Du, A., 2010. In-situ U-Pb, Hf and Re–Os isotopic analyses of the Xiangshan Ni–Cu–Co deposit in Eastern Tianshan (Xinjiang), Central Asia Orogenic Belt: constraints on the timing and genesis of the mineralization. Lithos 120 (3), 547–562.
Han, C., Xiao, W., Zhao, G., Su, B.X., Ao, S.J., Zhang, J., Wan, B., 2013. Age and tectonic setting of magmatic sulfide Cu-Ni mineralization in the Eastern Tianshan Orogenic Belt, Xinjiang, Central Asia. J. Geosci. 58 (3), 233–250.
Hiebert, R.S., Bekker, A., Wing, B.A., Rouxel, O.J., 2013. The Role of paragneiss assimilation in the origin of the Voisey's Bay Ni-Cu sulfide deposit, labrador: multiple S and Fe isotope evidence. Econ. Geol. 108 (6), 1459–1469.
Holwell, D.A., Boyce, A.J., Nald, I., 2007. Sulfur isotope variations within the Platreef Ni-Cu-PGE deposit: genetic implications for the origin of sulfide mineralization. Econ. Geol. 102 (6), 1091–1110.
Hu, A., Wang, Z., Tu, G., 1997. Geological Evolution and Diagenic and Metallogenetic Regularity in Northern Xinjiang. Science Press, Beijing pp 230. (in Chinese).
Hulston, H.J., Thode, T.H., 1965. Variations in the S^{33}, S^{34}, and S^{36} contents of meteorites and their relation to chemical and nuclear effects. J. Geophys. Res. 70 (14), 3475–3484.
Jiang, C., Cheng, S., Ye, S., Xia, M., Jiang, H., Dai, Y., 2006. Lithogeochemistry and petrogenesis of Zhongposhanbei maric rock body, at Beishan region Xinjiang. Acta Petrol. Sin. 22 (1), 115–126 (in Chinese with English abstract).
Jiang, C.Y., Guo, N.X., Xia, M.Z., Ling, J.L., Guo, F.F., Deng, X.Q., Jiang, H.B., Fan, Y.Z., 2012. Petrogenesis of the Poyi mafic-ultramafic layered intrusion, NE Tarim Plate. Acta Petrol. Sin. 28 (7), 2209–2223 (in Chinese with English abstract).
Labidi, J., Cartigny, P., Moreira, M., 2013. Non-chondritic sulphur isotope composition of the terrestrial mantle. Nature 501 (7466), 208–211.
Lehmann, J., Arndt, N., Windley, B., Zhou, M.F., Wang, C.Y., Harris, C., 2007. Field relationships and geochemical constraints on the emplacement of the Jinchuan intrusion and its Ni-Cu-PGE sulfide deposit, Gansu, China. Econ. Geol. 102 (1), 75–94.
Li, C., Ripley, E.M., 2009. Sulfur contents at sulfide-liquid or anhydrite saturation in silicate melts: empirical equations and example applications. Econ. Geol. 104 (3), 405–412.
Li, H., Chen, F., Mei, Y., Wu, H., Cheng, S., Yang, J., Dai, Y., 2006. Isotopic ages of No. 1 intrusive body in Pobei mafic-ultramafic belt of Xinjiang and their geological significance. Miner. Deposits 25 (4), 463 (in Chinese with English abstract).
Lightfoot, P.C., Hawkesworth, C.J., 1997. Flood basalts and magmatic Ni, Cu, and PGE sulphide mineralization: comparative geochemistry of the Noril'sk (Siberian Traps) and West Greenland sequences: Large igneous provinces: continental, oceanic, and planetary flood volcanism. pp. 357–380.
Liu, H.B., Jin, G.S., Li, J.J., Han, J., Zhang, J.F., Zhang, J., Zhong, F.W., Guo, D.Q., 2013. Determination of stable isotope composition in uranium geological samples. World Nuclear Geosci. 30 (3), 174–179 (in Chinese with English abstract).
Liu, Y., Samaha, N.T., Baker, D.R., 2007. Sulfur concentration at sulfide saturation (SCSS) in magmatic silicate melts. Geochim. Cosmochim. Acta 71 (7), 1783–1799.
Liu, Y.G., 2015. Diagenesis-mineralization of Copper-Nickel deposits and prospecting indicators in Pobei area, Xinjiang. The Dissertation for the Doctor Degree of China University of Geosciences (Wuhan). pp 1–170. (in Chinese with English abstract).
Liu, Y.G., Lv, X.B., Yang, L.S., Wang, H., Meng, Y., Yi, Q., Zhang, B., Wu, J., Ma, J., 2015. Metallogeny of the Poyi magmatic Cu-Ni deposit: revelation from the contrast of PGE and olivine composition with other Cu-Ni sulfide deposits in the Early Permian, Xinjiang, China. Geosci. J. 19 (4), 613–620.
Liu, Y.G., Lü, X.B., Wu, C.M., Hu, X., Duan, Z., Deng, G., Wang, H., Zhu, X., Zeng, H., Wang, P., 2016. The migration of Tarim plume magma toward the northeast in Early Permian and its significance for the exploration of PGE-Cu-Ni magmatic sulfide deposits in Xinjiang, NW China: as suggested by Sr-Nd-Hf isotopes, sedimentology and geophysical data. Ore Geol. Rev. 72, 538–545.
Liu, Y.G., Li, W.Y., Lü, X.B., Huo, Y.H., Zhang, B., 2017. The Pobei Cu-Ni and Fe ore deposits in NW China are comagmatic evolution products evidence from ore microscopy, zircon U-Pb chronology and geochemistry. Geologica Acta 15 (1), 37–50.
Lyons, J.R., 2007. Mass-independent fractionation of sulfur isotopes by isotope-selective photodissociation of SO_2. Geophys. Res. Lett. 34 (22), 1–5. http://dx.doi.org/10.1029/2007GL031031.
Mao, J.W., Pirajno, F., Zhang, Z.H., Chai, F.M., Wu, H., Chen, S.P., Cheng, L.S., Yang, J.M., Zhang, C.Q., 2008. A review of the Cu–Ni sulphide deposits in the Chinese Tianshan and Altay orogens (Xinjiang Autonomous Region, NW China): principal characteristics and ore-forming processes. J. Asian Earth Sci. 32 (2), 184–203.
Mao, J.W., Yang, J.M., Qu, W.J., Du, A.D., Wang, Z.L., Han, C.M., 2003. Re-Os Age of Cu-Ni Ores from the Huangshandong Cu-Ni Sulfide Deposit in the East Tianshan Mountains and Its Implication for Geodynamic Processes. Acta Geol. Sin.-Engl. 77 (2), 220–226.
Mavrogenes, J.A., O'Neill, H.S.C., 1999. The relative effects of pressure, temperature and oxygen fugacity on the solubility of sulfide in mafic magmas. Geochim. Cosmochim. Acta 63 (7), 1173–1180.
Miller, J.D., 1999. Information Circular 44. Geochemical Evaluation of Platinum Group Element (PGE) Mineralization in the Sonju Lake Intrusion, Finland, Minnesota.
Naldrett, A.J., 2004. Fundamentals of magmatic sulfide deposits. Rev. Econ. Geol. 17, 1–50.
Ohtani, E., Kawabe, I., Moriyama, J., Nagata, Y., 1989. Partitioning of elements between majorite garnet and melt and implications for petrogenesis of komatiite. Contrib. Miner. Petrol. 103 (3), 263–269.
Park, Y.R., Ripley, E.M., Miller, J.D., Li, C., Mariga, J., Shafer, P., 2004. Stable isotopic constraints on fluid-rock interaction and Cu-PGE-S redistribution in the Sonju Lake Intrusion, Minnesota. Econ. Geol. 99 (2), 325–338.
Peach, C., Mathez, E., Keays, R., 1990. Sulfide melt-silicate melt distribution coefficients for noble metals and other chalcophile elements as deduced from MORB: implications for partial melting. Geochim. Cosmochim. Acta 54 (12), 3379–3389.
Penniston-Dorland, S.C., Mathez, E.A., Wing, B.A., Farquhar, J., Kinnaird, J.A., 2012. Multiple sulfur isotope evidence for surface-derived sulfur in the Bushveld complex. Earth Planet. Sci. Lett. 337, 236–242.
Pirajno, F., Ernst, R.E., Borisenko, A.S., Fedoseev, G., Naumov, E.A., 2009. Intraplate magmatism in Central Asia and China and associated metallogeny. Ore Geol. Rev. 35 (2), 114–136.
Pirajno, F., Mao, J.W., Zhang, Z.C., Zhang, Z.H., Chai, F.M., 2008. The association of mafic-ultramafic intrusions and A-type magmatism in the Tian Shan and Altay orogens, NW China: implications for gedodynamic evolution and potential for the discovery of new ore deposits. Asian J. Earth Sci. 32 (2), 165–183.
Qin, K.Z., Li, X.M., 2011. Large mafic-ultramafic copper-nickel deposit forecasts and target Assessment project number: 2006BAB07B03 commitment undertake: Institute of Geology and Geophysics. Chinese academy of sciences, pp. 515 (In Chinese).
Qin, K.Z., Su, B.X., Sakyi, P.A., Tang, D.M., Li, X.H., Sun, H., Xiao, Q.H., Liu, P.P., 2011. SIMS zircon U-Pb geochronology and Sr-Nd isotopes of Ni-Cu-Bearing Mafic-Ultramafic Intrusions in Eastern Tianshan and Beishan in correlation with flood basalts in Tarim Basin (NW China): constraints on a ca. 280 Ma mantle plume. Am. J. Sci. 311 (3), 237–260.
Ripley, E.M., Li, C., 2013. Sulfide saturation in mafic magmas: is external sulfur required for magmatic Ni-Cu-(PGE) ore genesis? Econ. Geol. 108 (1), 45–58.
Roeder, P., Emslie, R., 1970. Olivine-liquid equilibrium. Contrib. Miner. Petrol. 29 (4), 275–289.
Rumble, D., 2005. Presidential Address to the mineralogical society of America Seattle, November 4, 2003 – A mineralogical and geochemical record of atmospheric photochemistry. Am. Mineral. 90 (5–6), 918–930.
Salters, V.J., Stracke, A., 2004. Composition of the depleted mantle. Geochem. Geophys. Geosyst. 5 (5), 469–484.
Sharman, E., Penniston-Dorland, S., Kinnaird, J., Nex, P., Brown, M., Wing, B., 2013. Primary origin of marginal Ni-Cu-(PGE) mineralization in layered intrusions: $\Delta^{33}S$ evidence from The Platreef, Bushveld, South Africa. Econ. Geol. 108 (2), 365–377.
SGTXBGMR (Sixth Geological Team of the Xinjiang Bureau of Geology and Mineral Resources), 2012. The Detailed Survey Report of Poyi Cu-Ni Deposit. Xinjiang, China, pp. 1–261.
Song, X.Y., Xie, W., Deng, Y.F., Crawford, A.J., Zheng, W.Q., Zhou, G.F., Deng, G., Cheng, S.L., Li, J., 2011. Slab break-off and the formation of Permian mafic–ultramafic intrusions in southern margin of Central Asian Orogenic Belt, Xinjiang, NW China. Lithos 127 (1), 128–143.
Stone, W., Crocket, J., Fleet, M., 1990. Partitioning of palladium, iridium, platinum, and gold between sulfide liquid and basalt melt at 1200 C. Geochim. Cosmochim. Acta 54 (8), 2341–2344.
Su, B.X., Qin, K.Z., Sakyi, P.A., Liu, P.P., Tang, D.M., Malaviarachchi, S.P., Xiao, Q.H., Sun, H., Dai, Y.C., Yan, H., 2011. Geochemistry and geochronology of acidic rocks in the Beishan region, NW China: petrogenesis and tectonic implications. J. Asian Earth Sci. 41 (1), 31–43.
Su, B.X., 2014. Mafic-ultramafic Intrusions in Beishan and Eastern Tianshan at Southern CAOB: Petrogenesis, Mineralization and Tectonic Implication. Springer, Berlin Heidelberg, pp. 1–209.
Sun, H., 2009. Ore-forming mechanism in conduit system and ore-bearing property evaluation for mafic–ultramafic complex in Eastern Tianshan, Xinjiang. Unpublished PhD thesis.
Sun, S.S., McDonough, W.F., 1989. Chemical and isotopic systematics of oceanic basalts: implications for mantle composition and processes. Geological Society, London, Special Publications 42 (1), 313–345.
Takahashi, E., 1978. Partitioning of Ni^{2+}, Co^{2+}, Fe^{2+}, Mn^{2+} and Mg^{2+} between olivine and silicate melts: compositional dependence of partition coefficient. Geochim. Cosmochim. Acta 42 (12), 1829–1844.
Tang, D.M., Qin, K.Z., Sun, H., Su, B.X., Xiao, Q.H., 2012. The role of crustal contamination in the formation of Ni–Cu sulfide deposits in Eastern Tianshan, Xinjiang, Northwest China: Evidence from trace element geochemistry, Re–Os, Sr–Nd, zircon Hf–O, and sulfur isotopes. J. Asian Earth Sci. 49 (3), 145–160.
Tao, Y., Li, C., Hu, R., Ripley, E.M., Du, A., Zhong, H., 2007. Petrogenesis of the Pt–Pd mineralized Jinbaoshan ultramafic intrusion in the Permian Emeishan large igneous province, SW China. Contrib. Miner. Petrol. 153 (3), 321–337.
Watanabe, Y., Farquhar, J., Ohmoto, H., 2009. Anomalous fractionations of sulfur isotopes during thermochemical sulfate reduction. Science 324 (5925), 370–373.
Wendlandt, R.F., 1982. Sulfide saturation of basalt and andesite melts at high pressures and temperatures. Am. Mineral. 67, 877–885.
Wu, H., Li, H., Mo, X., Chen, F., Lu, Y., Mei, Y., Deng, G., 2005. Age of the Baishiqun mafic-ultramafic complex, Hami, Xinjiang and its geological significance. Acta Geologica Sinica – Chinese Edition 79 (4), 498 (in Chinese with English abstract).
Wykes, J.L., O'Neill, H.S.C., Mavrogenes, J.A., 2015. The Effect of FeO on the Sulfur Content at Sulfide Saturation (SCSS) and the Selenium Content at Selenide Saturation of Silicate Melts. J. Petrol. 56 (7), 1407–1420.
Xia, M.Z., Jiang, C.Y., Li, C., Xia, Z.D., 2013. Characteristics of a Newly Discovered Ni-Cu Sulfide Deposit Hosted in the Poyi Ultramafic Intrusion, Tarim Craton, NW China. Econ. Geol. 108 (8), 1865–1878.
Xiao, P.X., 2004. 1:200000 district geological Survey report of BiJiashan, pp. 315. (in Chinese).
Xiao, W.J., Zhang, L.C., Qin, K.Z., Sun, S., Li, J.L., 2004. Paleozoic accretionary and

collisional tectonics of the Eastern Tianshan (China): implications for the continental growth of central Asia. Am. J. Sci. 304 (4), 370–395.
Xu, X., He, S., Wang, H., Chen, J., 2009. Geological Background Map of Mineralization in Eastern Tianshan-Beishan Area. Geological Publishing House, Beijing (in Chinese).
Xue, S., Qin, K., Li, C., Tang, D., Mao, Y., Qi, L., Ripley, E.M., 2016. Geochronological, Petrological, and Geochemical Constraints on Ni-Cu Sulfide Mineralization in the Poyi Ultramafic-Troctolitic Intrusion in the Northeast Rim of the Tarim Craton, Western China. Econ. Geol. 111 (6), 1465–1484.
Yang, H., Li, Y., Li, W., Yang, J., Zhao, G., Sun, N., Wang, X., Tan, W., 2008. General discussion on metallogenetic tectonic setting of Beishan mountain, northwestern China. Northwestern Geol. 41, 22–28 (in Chinese with English abstract).
Yang, S., 2011. The Permian Pobei mafic-ultramafic intrusion (NE Tarim, NW China) and associated sulfide mineralization. The University of Hong Kong (Pokfulam, Hong Kong). pp 1–365.
Yang, S.H., Zhou, M.F., Lightfoot, P.C., Xu, J.F., Wang, C.Y., Jiang, C.Y., Qu, W.J., 2014. Re–Os isotope and platinum-group element geochemistry of the Pobei Ni–Cu sulfide-bearing mafic–ultramafic complex in the northeastern part of the Tarim Craton. Miner. Deposita 49 (3), 381–397.
Yu, H., Lu, S., Mei, H., Zhao, F., Li, H., Li, H., 1999. Characteristics of Neoproterozoic eclogite-granite zones and deep level ductile shear zone in western China and their significance for continental reconstruction. Acta Petrol. Sin. 15 (4), 532–538 (in Chinese with English abstract).
Zhang, M., Li, C., Fu, P., Hu, P., Ripley, E.M., 2011. The Permian Huangshanxi Cu–Ni deposit in western China: intrusive–extrusive association, ore genesis, and exploration implications. Miner. Deposita 46 (2), 153–170.
Zhang, M.J., Tang, Q.Y., Cao, C.H., Li, W.Y., Wang, H., Li, Z.P., Yu, M., Feng, P.Y., 2017. The origin of Permian Pobei ultramafic complex in the northeastern Tarim craton, western China: evidences from chemical and C-He-Ne-Ar isotopic compositions of volatiles. Chem. Geol. http://dx.doi.org/10.1016/j.chemgeo.2017.06.006.
Zheng, Y.F., Chen, J.F., 2000. Stable Isotope Geochemistry. Science Press, Beijing pp 136. (in Chinese).
Zhou, M.F., Michael, L.C., Yang, Z., Li, J., Sun, M., 2004. Geochemistry and petrogenesis of 270 Ma Ni–Cu–(PGE) sulfide-bearing mafic intrusions in the Huangshan district, Eastern Xinjiang, Northwest China: implications for the tectonic evolution of the Central Asian orogenic belt. Chem. Geol. 209 (3), 233–257.